5.55

SIMULATED EFFECTS OF AN ISOLATED SUPERCELL ON THE EVOLUTION OF A NEARBY SQUALL LINE

Jacey Wipf* and Adam French
South Dakota School of Mines and Technology

1. INTRODUCTION

Operational forecasters often have to try to anticipate how thunderstorms and their associated hazards will evolve over time. One scenario where this can be particularly challenging is when several convective storm types are present in the vicinity of each other.

A number of past studies have investigated cases where neighboring storms merge into a single storm system. A common outcome is that storm mergers often cause a transition from one storm type to another, such as from a supercell to a bow echo, as described in Klimowski et al. (2003) and Finley et al. (2001). French and Parker (2012) documented the evolution of squall lines in cases where they merged with isolated supercells, finding that storm rotation weakened, hail production declined, and damaging winds increased following the merger. French and Parker (2014) were able to further isolate the role of these types of storm mergers in bow echo development.

Storms interacting with mesoscale boundaries have also shown similar results in storm evolution. Past studies have documented how mesoscale boundaries interact with nearby storm types, including acting as sources of low-level vorticity (Markowski et al. 1998) that produce suitable conditions for tornadogenesis (Wolf et al. 1996, Sabones et al. 1996).

The current study examines a squall line in the vicinity of an isolated supercell, and the effects the supercell's cold pool boundary has on the evolution of the squall line. This interaction is hypothesized to lead to heterogeneity along the squall line, such as bowing segments and mesovortex development, which may lead to more severe weather. A series of sensitivity tests was performed in order to distinguish the effects of supercell proximity to the squall line and the positioning of the supercell relative to the squall line.

* *Corresponding author address:* Jacey Wipf, South Dakota School of Mines and Technology, Atmospheric and Environmental Sciences Program, Rapid City, SD 57701; e-mail: jacey.wipf@mines.sdsmt.edu.

2. METHODOLOGY

This study utilizes version 1.17 of the Bryan cloud model (CM1, Bryan and Fritsch 2002) to examine the effects that an isolated supercell has on a nearby squall line. CM1 is a three-dimensional, non-hydrostatic, nonlinear, numerical model intended for idealized studies such as the series of tests discussed below. A horizontal grid spacing of 500 m (and in some cases 750 m) and a vertical grid spacing of 250 m were chosen in order to sufficiently resolve convective scale processes (Bryan et al. 2003) while keeping computational expense manageable. The idealized thermodynamic profile described in Weisman and Klemp (1982) and a pair of wind profiles based off Rotunno et al. (1988) and Weisman and Klemp (1984) were implemented to simulate two distinct convective storm organizations. Additional details of the model configuration are described in Table 1.

Squall lines and supercells require two different environments to organize efficiently. In order to examine the interaction between them in CM1, the Instant Base-State Substitution (I-BSS) method described by Letkewicz et al. (2013) was used to simulate both storm types within a single model domain. The model run was initialized with a representative squall line sounding and elongated positive temperature perturbation in order to simulate a squall line. The model was run for approximately three hours, allowing the squall line to develop and the cold pool to strengthen. Then the background wind profile was replaced with one favoring an isolated supercell, while the squall line-induced perturbations remain intact. Another smaller, warm bubble was added ahead of the squall line to trigger an isolated supercell, and the simulation continued for another three hours to allow the two storms to interact.

A series of sensitivity tests was performed to examine the varying effects the supercell can have on the squall line. We investigated four supercell proximity locations, including 50, 75, 100, and 125 km ahead of the squall line's cold pool (Figure 1). Each location site was centered on the squall line's apex (y = 150 km).

Another set of tests included differing supercell locations along the squall line at a constant distance of 100 km ahead of the squall line's cold pool. Starting at the apex, three locations north and three locations south, each spaced 40 km apart, were simulated (Figure 1).

3. RESULTS AND DISCUSSION

3.1 *Squall Line-No Supercell Tests*

We will begin our analysis with a discussion of a control run that consisted of just the squall line simulated without the added supercell. This simulation included the change in wind profile after three hours and provides a benchmark to which we can compare the effects of the various supercell runs discussed below.

Cold Pool Evolution:

Once the cold pool is established, it initially grows laterally in the x-direction. After two hours, the apex region, defined as the center of bowing, of the squall line's cold pool strengthens and begins to extend forward. At three hours, the cold pool extends ahead of the convective region and is strongest at the apex, with the north and south ends being comparatively warmer. After the restart, the cold pool apex region strengthens further, the ends remain warm, and as a whole, the cold pool continues expanding.

After one hour, a strong gust front updraft (w greater than 5 m s^{-1}) develops along the entire leading edge of the cold pool. As the simulation continues and even after the restart, the gust front lifting about the apex region remains strong and intact, whereas the gust front lifting towards the north and south ends weakens and becomes segmented.

Mesovortex Development:

There are several clusters of weak mesovortices (referring to areas of semi-persistent positive vertical vorticity) embedded within the squall line for the entire simulation. Mesovortex activity increases as the cold pool strengthens, and there are stronger signatures slightly north of the apex compared to slightly south of the apex. This is consistent with past studies of mesovortices in squall lines (e.g. Weisman and Trapp 2003).

Simulated Radar Structure:

The squall line appears very cellular in nature from the beginning. A stratiform region begins to form behind the convective region, and the line begins to bow after two hours. After three hours, there is a transition from a trailing stratiform to a leading stratiform squall line, most likely in response to the stronger wind shear environment (Parker and Johnson 2004). The squall line continues to bow, and the convective areas in the north and south ends become disconnected from the main squall line body.

3.2 *Proximity Tests*

The effects of the distance between the squall line and the supercell on storm evolution were investigated through four sensitivity tests known as the "proximity tests." After three hours of squall line growth, a supercell was introduced at different distances from the squall line. All of these tests had the same y-coordinate, being aligned with the apex of the squall line, but varying x-coordinates, corresponding to 50, 75, 100, and 125 km ahead of the squall line's cold pool (Figure 1). By keeping one coordinate constant, we were able to consider the effects of introducing the supercell at different proximities. These tests also allow us to examine the role of the supercell's maturity. The closer the distance, the less time the supercell had to mature, and vice versa.

Cold Pool Evolution:

In all four cases the squall line's cold pool was observed to weaken as it encountered the supercell's cold pool (an example of this observed weakening is shown in the 75 km proximity case depicted in Figure 2b). Another common observation is the development of a bulge in the squall line's cold pool after the convective regions (defined by simulated radar reflectivity greater than 40 dBZ) in both storms merged (Figure 2c). We will hereafter refer to this as the "reflectivity merge," which often differed from when the cold pools collided, which is the primary focus of this study.

Although all four cases share similar evolutionary characteristics, the degree to which the weakening occurs as well as the size, strength, and number of cold pool bulges vary as the distance and maturity of the supercell varies. At 50 km away, the supercell has very little time to develop and organize as well as produce a mature cold pool. Before the reflectivity merge, there was minimal weakening in the squall line's cold pool. However, once the convective regions merged, weakening in the squall line did occur and continued throughout the model run. The squall line's cold pool strengthened around the supercell, and created two small bulges to the north and south of the supercell (Figure 3d).

At 75 and 100 km away, the supercell had more time to mature and produce a strong cold pool. These two cases were very similar, in the sense that the squall line's cold pool weakened at the onset of the cold pools merging, and continued to weaken during the reflectivity merge (Figure 2a-c). They were dissimilar in the sense that after the reflectivity merge, the 75 km run developed two cold pool bulges, a stronger one to the north and a weaker one to the south (Figure 2c), whereas the 100 km run only produced a weak cold pool bulge to the north (Figure 3e). The 125 km run had the largest supercell cold pool by the time of the merge. This resulted in the largest magnitude and area of squall line cold pool weakening (Figure 3f), as well as a weak cold pool bulge to the north.

There were also common patterns in the gust front lifting observed in all four cases. As the squall line and supercell's cold pools collided, the squall line's gust front, initially characterized by an intense line of upward motion, diminishes (Figure 2e). After the reflectivity merge, however, a new gust front develops at the forefront of the merged storms (Figure 2f). This pattern of behavior is consistent with a recent study of squall line-supercell mergers by French and Parker (2014).

As with overall cold pool intensity, the effects of gust front lifting varied with the distance of the supercell from the squall line. When the supercell originated in close proximity (e.g. the 50 km case) it had less time to mature and produce cold outflow, and the weakening on the gust front lifting was minimal. As the distance between the storms increases, and the supercell's cold pool has more time to strengthen, the weakening quickens at the onset of the cold pool collision, as seen in the 75 km case depicted in Figure 2.

After a certain distance, however, this pattern was not as pronounced. For instance, significant weakening of the squall line's gust front lifting was observed in the 100 and 125 km cases, but it does not completely dissolve until after the reflectivity merge. This appears to be the result of the squall line's cold pool also strengthening over time (primarily due to the intensified convection owing to the stronger sheared environment), prior to encountering the supercell's outflow.

Another feature in these last two cases is a more discontinuous new gust front that develops around the newly merged storms. It appears that as the distance increases in these model runs, the post-merge gust front does not fully redevelop, in terms of a continuous uniform swath of vertical ascent. An example of the discontinuous swath of gust front lifting is shown in the 100 km proximity case depicted in Figure 4. This figure shows several areas of decreased upward velocity along the leading edge (indicated by the ovals in the figure), compared to the fully-redeveloped, continuous line of gust front lifting shown in Figure 2f.

Mesovortex Development:

In all cases, there is mesovortex activity embedded in the squall line and low-level circulation present in the supercell prior to the cold pools interacting. Unlike the cold pool and gust front features, there is no clear relationship between the proximity/supercell cold pool strength and mesovortex development.

In the 50 km case, the low-level circulation in the supercell is minimal, due to the small amount of time the supercell has had to mature prior to merging (Figure 5g). However, as the cold pools collide, several mesovortices develop, including a strong mesovortex along the interface of the squall line-supercell interaction that persists for twenty minutes (Figure 5h). Also, a preexisting mesovortex embedded in the squall line is greatly enhanced as the cold pools collide, and persists for nearly forty minutes (Figure 5i). None of the other sensitivity tests (in both sets of proximity and position tests) produced mesovortices this isolated or persistent.

In the 75 km case, as the cold pools collide, several distinct mesovortices develop within the squall line. In the 100 km case, as the cold pools collide, the low-level circulation within the supercell diminishes as the mesovortices in the squall line temporarily intensify and then rapidly dissipate. In the 125 km case, however, the low-level circulation in the supercell remains intact and no new mesovortices in the squall line develop. The different processes responsible for the variable mesovortex evolutions are still being investigated.

Simulated Radar Structure:

In all cases, as the supercell's cold pool encroaches on the region of leading stratiform in the squall line, the reflectivity decreases (Figure 2a). Where cold pool bulges were observed, corresponding bowing segments were found in the simulated radar field.

In all but the 50 km case, before the reflectivity merge the squall line begins to transition from a continuous line of convection to a more broken swath. Because of the cellular nature of this squall line, the bowing segments are short and inconsistent (Figure 6). In the 50 km case, the line is rather unbroken before the reflectivity merge, and bowing segments are more obvious and correspond to the cold pool bulges. The evolution seen in the 50 km case is most similar to the evolution in the merger simulations described by French and Parker (2014), who used an x-distance of 60 km between their squall line and supercell.

3.3 *Position Tests*

The placement of the supercell along the squall line was investigated through 7 sensitivity tests known as the "position tests." After three hours of squall line growth, similar to the proximity tests, a supercell was added at different locations along the squall line. All of these tests had approximately 100 km between the cold pool of the squall line and the supercell, but the supercell was placed at 40 km increments along the leading edge of the squall line's cold pool (Figure 1). By keeping the distance between the squall line and supercell constant, we were able to isolate only the effects of the supercell at different positions along the squall line.

Cold Pool Evolution:

Similar to the proximity model simulations, in almost every case, the interaction between the cold pools led to a weakening in the squall line's cold pool strength (Figure 2b). Cold pool bulges were also observed along the squall line after the reflectivity merge (Figure 2c). However, the degree and extent of the weakening and bulge formations differed in each case.

Generally, if the supercell-squall line interaction occurred to the north of the apex of the squall line, the squall line's cold pool weakened at the onset of interaction, while the southern portion remained intact. The cold pool bulge would then form south of the merge, usually near the apex. If the interaction occurred south of the apex, the squall line's cold pool weakened at the onset, but generally to a lesser degree than cases further north. The bulge formed to the north of the interaction, still near the apex, and no real generalization can be made about the bulge's strength compared to the northern set.

There also seemed to be a relationship between cold pool characteristics and the distance from the interaction to the apex. The closer the cold pools collided to the apex, whether it's to the north or south, the more dramatic the cold pool weakening, and the stronger the cold pool bulge. At the far ends of the tested supercell locations, such as the 270 and 30 cases, the supercell cold pool had less of an effect on the squall line because both cold pools had relatively similar temperatures at these locations, and therefore the weakening was minimal. Although the rest of the squall line's cold pool remained strong, there was no major bulge that developed (the 30 case is depicted in Figure 3c).

The 150 case (which is also the same as the 100 km proximity case) shows a rather large area within the squall line's cold pool where weakening occurred. The cold pool bulge formed to the north, similar to the southern sets, and was rather weak compared to some of the other position tests (Figure 3e). The 190 and 230 cases (both northern tests) are similar, with comparable strong cold pool bulges and substantial weakening within the squall line at the onset of the cold pool merge (the 230 case is shown in Figure 3a). The 110 and 70 cases (both southern tests) deviate slightly from the generalizations, such that in the 110 case the cold pool bulge that forms after the reflectivity merge is perhaps the strongest (coldest temperatures over a large area) of all the runs (Figure 3b), and the 70 case shows the largest (but not nearly as strong) cold pool bulge.

In all of the position cases, and similarly to the proximity tests, the squall line gust front lifting diminished as it interacted with the supercell's cold pool (Figure 2e). Then, after the reflectivity merge, a new gust front developed around the newly merged storms (Figure 2f). However, the pace of the weakening and the uniformity of the new leading edge differed in each case.

In the northern cases, the squall line's gust front weakened faster, usually before the reflectivity merge. The southern cases display a slower dissipation of the gust front, often not completely dissolving until after the reflectivity merge. For the interactions close to the apex, the initial gust front was completely replaced by a new one that formed after the reflectivity merge. As the distance between the apex and interaction increases, there is less redevelopment of the squall line gust front after the merge, and the line is more discontinuous, much like the 100 and 125 proximity cases.

Again, the centered 150 case is similar to the southern sets, such that the squall line's gust front weakens slowly and doesn't diminish until after the reflectivity merge, at which point the new gust front develops, but with discontinuous segments.

Mesovortex Development:

In all cases, there is mesovortex activity embedded in the squall line and low-level circulation present in the supercell prior to the cold pools interacting. Unlike the cold pool and gust front features, there is no clear relationship between the supercell position and mesovortex development.

In the northern sets, the right mover supercell, which is more updraft dominated due to the wind profile, intercepts the squall line. In these cases, the supercell develops a strong and consistent low-level circulation that eventually interacts with the squall line. In the southern sets, the left mover supercell, which is more downdraft dominated, intercepts the squall line. There is little to no strong preexisting low-level circulation within these supercells before interacting with the squall line.

For the cases near the apex (110, 150, and 190), the preexisting mesovortices are enhanced at the interface of the squall line-supercell cold pool interaction, but none are very strong or persistent (the 110 case is shown in Figure 5a-c). At the far ends of the squall line (270 and 30), there are few to no mesovortices in the squall line throughout the simulation. However, the in between cases (230 and 70) don't seem to show any recognizable patterns. The 70 case shows no mesovortex development prior to the reflectivity merge, and the mesovortices that do develop are relatively weak and transient. In the 230 case, the right mover supercell develops a region of very strong low-level circulation that enhances the mesovortex development along the interface of the cold pool merge (Figure 5d-f).

Simulated Radar Structure:

Very similar to the observations in the proximity tests, as the cold pool encroaches on the leading stratiform region in the squall line, the reflectivity decreases (Figure 2a). Before the reflectivity merge occurs, the squall line begins to transition from a continuous line of convection to a more broken swath. Due to the cellular nature of this squall line, the bowing segments are short and inconsistent. In the majority of the cases, most of the bowing segments that develop seem to correspond to the cold pool bulges. There are notable bowing segments in two cases; there is a small bowing segment north of the interaction in the 110 case and a distinct bowing segment near the apex in the 190 case (Figure 6).

4. FUTURE WORK

The present study investigated the effects of an isolated nearby supercell on the evolution of a squall line. This was done through a series of sensitivity tests examining the proximity between a squall line and supercell and the position of a supercell relative to a squall line. However, there are three more major sets of sensitivity tests planned for this investigation.

Firstly, the timing of the interactions will be examined by implementing the supercell temperature perturbation bubble at different times. Currently, the bubble is introduced at three hours into the squall line's lifecycle. We would like to look at least one hour before and one hour after this current time. The sooner the supercell is added, the less time the squall line has to develop, meaning the cold pool may not be as strong and be more susceptible to manipulation. Whereas, the later the supercell is added, the more time the squall line's cold pool has had time to strengthen and perhaps overtake the supercell's outflow. This type of sensitivity test will be a counterpart to the proximity tests described above. Instead of testing the different levels of maturity in the supercell, we will be testing the different levels of maturity in the squall line. If one of these scenarios shows interesting development, more sensitivity tests may be run.

The second set of tests include differing types of supercells, in regards to low precipitation (LP), classic (C), and high precipitation (HP). These precipitation schemes will be determined through the moisture content throughout the vertical column. There are several ways to do this in CM1, but we plan on implementing different atmospheric soundings representing documented typical cases of the LP, C, and HP environments. The main goal of these tests is to see how the effects of different cold pool structures (which are generally observed with different supercell types) will impact squall line evolution.

Finally, a set of tests will be performed to investigate the effects of Coriolis on a select number of previously run position tests (keeping in mind that all the previous model simulations did not include Coriolis effects). These position tests include the 110, 150, and 190 cases, and were chosen because the interactions local to the apex region are hypothesized to have the largest effects. These tests will use the same parameters as the original tests, but with the Coriolis accelerations included. We will also need to modify the initial supercell bubble location because the Coriolis force changes the motion of the storms, resulting in the supercell-squall line interaction occurring at a different location along the squall line. To improve the outcome of these tests, we plan to initiate the supercell bubble at a more northward location, so that by the time the two storms interact, it will be in the same general region as its corresponding non-Coriolis test.

As a counterpart to the squall line-no supercell test, we would like to run a supercell-no squall line test to observe the evolution of an isolated supercell in the same environment. This sort of test will not include the I-BSS method, but rather will use a simpler technique of just implementing a supercell in the representative supercell environment used in all the model runs (excluding the LP, C, and HP supercell tests). By doing so, we will be able to compare the evolution of this lone supercell to the evolution of a supercell in the vicinity of a squall line, as well as, justify that the effects observed are a result of the cold pools interacting, not at artifact of the supercell evolution.

Once this sequence of model simulations is complete, we should have a better understanding of how interactions between neighboring storms may impact severe weather.

5. REFERENCES

Bryan, G. H. and J. M. Fritsch, 2002: A benchmark simulation for moist nonhydrostatic numerical models. *Mon. Wea. Rev.*, **130**, 2917–2928.

Bryan, G. H., J. Wyngaard, and J. M. Fritsch, 2003: Resolution requirements for the simulation of deep moist convection. *Mon. Wea. Rev.,* **131,** 2394-2416.

Finley, C. A., W. R. Cotton, and R. A. Pielke Sr., 2001: Numerical simulation of tornadogenesis in a high-precipitation supercell. Part I: Storm evolution and transition into a bow echo. *J. Atmos. Sci.*, **58**, 1597–1629.

French, A. J. and M. D. Parker, 2012: Observations of mergers between squall lines and isolated supercell thunderstorms. *Wea. Forecasting*, **27**, 255–278.

French, A. J. and M. D. Parker, 2014: Numerical simulations of bow echo formation following a squall line-supercell merger. *Mon. Wea. Rev.,* **142,** 4791-4822.

Klimowski, B. A., M. J. Bunkers, M. R. Hjelmfelt, and J. N. Covert, 2003: Severe convective windstorms over the Northern High Plains of the United States. *Wea. Forecasting*, **18**, 502–519.

Letkewicz, C. E., A. J. French, and M. D. Parker, 2013: Base-state substitution: An idealized modeling technique for approximating environmental variability. *Mon. Wea. Rev.*, **141**, 3062–3086.

Markowski, P. M., E. N. Rasmussen, and J. M. Straka, 1998: The occurrence of tornadoes in supercells interacting with boundaries during VORTEX-95. *Wea. Forecasting*, **13**, 852–859.

Parker, M. D. and R. H. Johnson, 2004: Simulated convective lines with leading precipitation. Part I: Governing dynamics. *J. Atmos. Sci.*,**61**, 1637–1655.

Rotunno, R., J. B. Klemp, and M. L. Weisman, 1988: A theory for strong, long-lived squall lines. *J. Atmos. Sci.*, **45**, 463–485.

Sabones, M., E. M. Agee, and M. Akridge, 1996: The Pulaski county and West Lafayette, Indiana tornadoes, 26-27 April 1994: A case of supercell (mesocyclone) and squall line bow-echo interaction. Preprints, *18th Conf. Severe Local Storms*, San Francisco, CA, Amer. Meteor. Soc.

Weisman, M. L. and J. B. Klemp, 1982: The dependence of numerically simulated convective storms on vertical wind shear and buoyancy. *Mon. Wea. Rev.*, **110**, 504–520.

Weisman, M. L. and J. B. Klemp, 1984: The structure and classification of numerically simulated convective storms in directionally varying wind shears. *Mon. Wea. Rev.*, **112**, 2479–2498.

Weisman, M. L. and R. J. Trapp, 2003: Low-level mesovortices within squall lines and bow echoes. Part I: Overview and dependence on environmental shear. *Mon. Wea. Rev.*, **131**, 2779–2803.

Wolf, R., R. Pryzbylinski, and P. Berg, 1996: Observations of a merging bowing segment and supercell. Preprints, *18th Conf. Severe Local Storms*, San Francisco, CA, Amer. Meteor. Soc.

Horizontal Grid Spacing	500 m, 750 m
Vertical Grid Spacing	250 m, stretched
Boundary Conditions	Free slip top and bottom Open north, south, east, and west
Microphysics	Thompson Scheme
Thermodynamic Profile	Weisman and Klemp (1982)
Wind Profile	Initial squall line sounding: Rotunno et al. (1988) Restart supercell sounding: Weisman and Klemp (1984)
Radiation, Coriolis, and Surface Fluxes	Neglected

Table 1: Current model configurations.

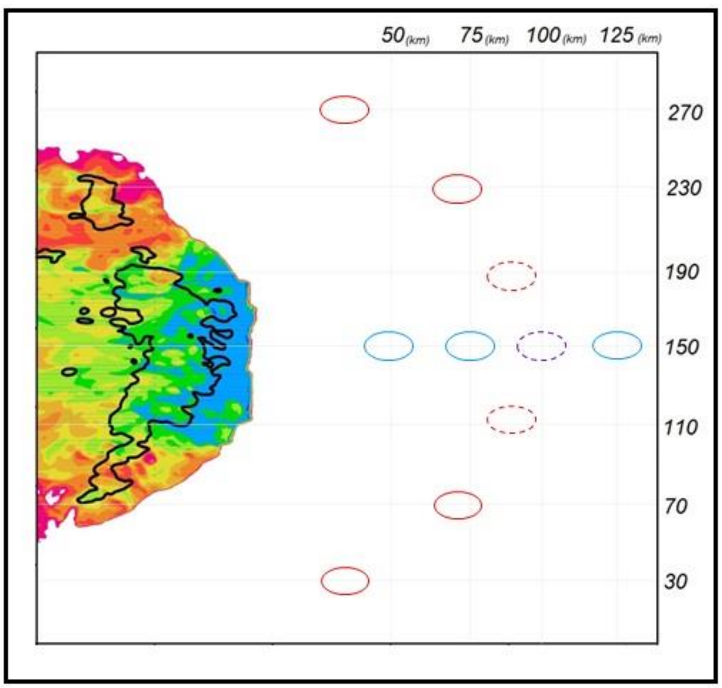

Figure 1: Schematic displaying the 10 supercell locations (indicated by the ovals) relative to the squall line's cold pool (indicated by the shading). The 4 proximity runs are shown in blue along the line denoted by y = 150, also referred to as the apex of the squall line, and spaced at 50, 75, 100, and 125 km away from the squall line's cold pool. The 7 position runs are shown in red and are spaced 100 km from the squall line's cold pool at 40 km increments apart (denoted by the numbers on the right). The purple oval is analyzed as both the 100 km proximity test and the 150 position test. The 3 dashed ovals indicate the Coriolis runs described under Future Work.

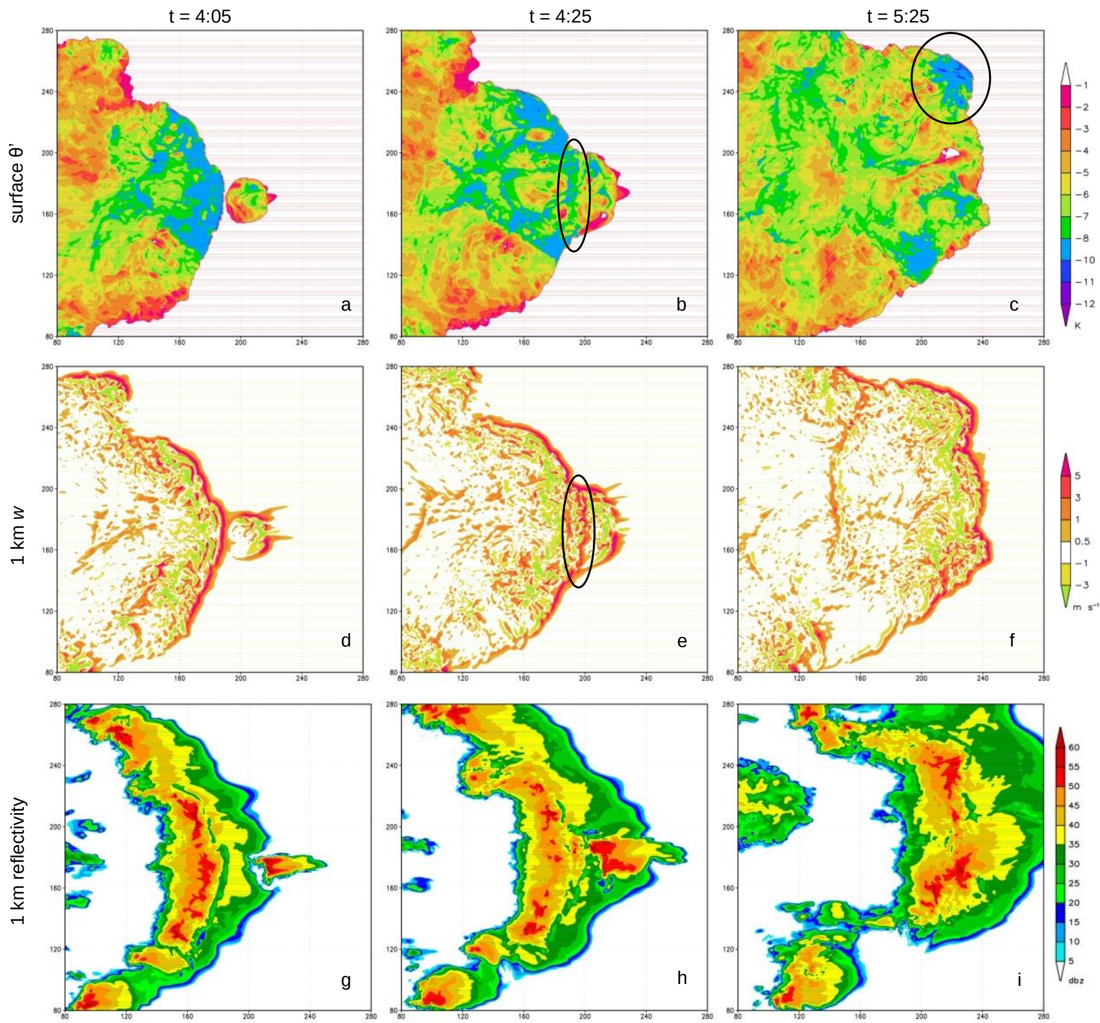

Figure 2: A time series of the 75 km proximity case showing the cold pool evolution denoted by shaded surface potential temperature perturbations (a-c), gust front lifting denoted by shaded 1 km AGL vertical velocity (d-f), and simulated radar reflectivity denoted by the shaded 1 km AGL dBZ (g-i). The black oval in 2b indicates the region of cold pool weakening at the interface of the cold pools merging, and corresponds to the black oval in 2e which indicates the gust front lifting diminishing. The black circle in 2c indicates a strengthening cold pool bulge.

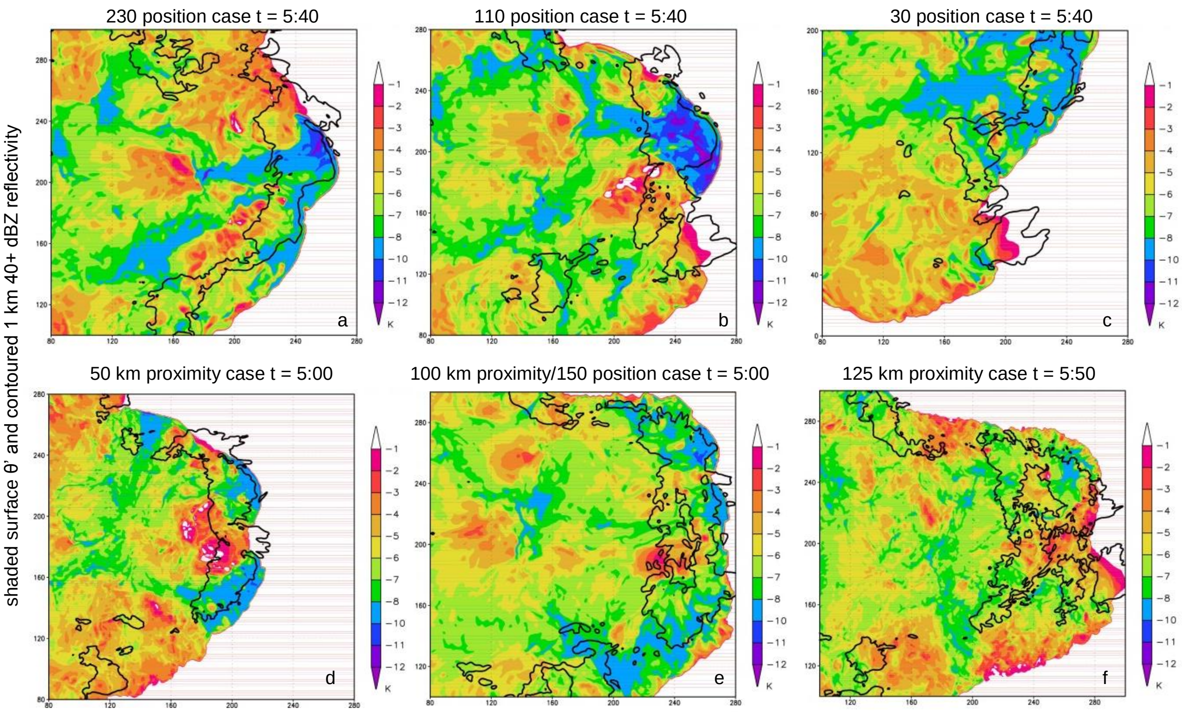

Figure 3: This figure shows the cold pool evolution, denoted by the shaded surface potential temperature perturbations, and convective regions (40+ dBZ) in simulated reflectivity fields, denoted by the black contours, in six separate cases. These cases include the 230 position (a), 110 position (b), 30 position (c), 50 km proximity (d), 100 km proximity / 150 position (e), and 125 km proximity (f).

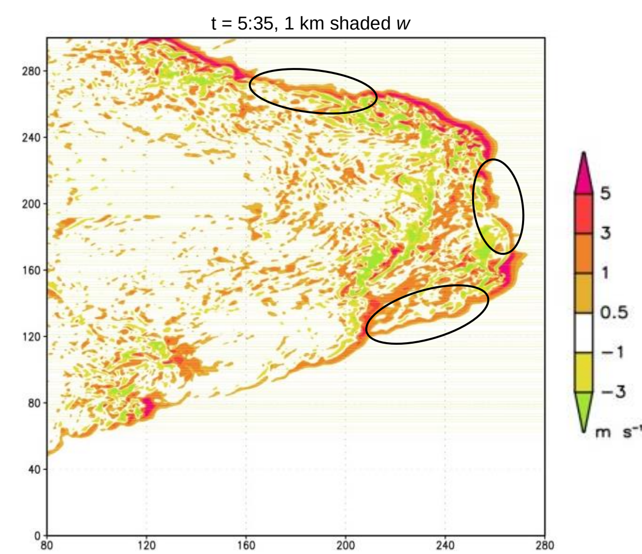

Figure 4: The 100 km proximity / 150 position case showing the new gust front redeveloping, denoted by shaded 1 km AGL vertical velocity, after the reflectivity merge. The leading edge is no longer a continuous line of ascent, but rather a line of discontinuous pockets of intense lifting. The black ovals indicate regions of weak gust front lifting.

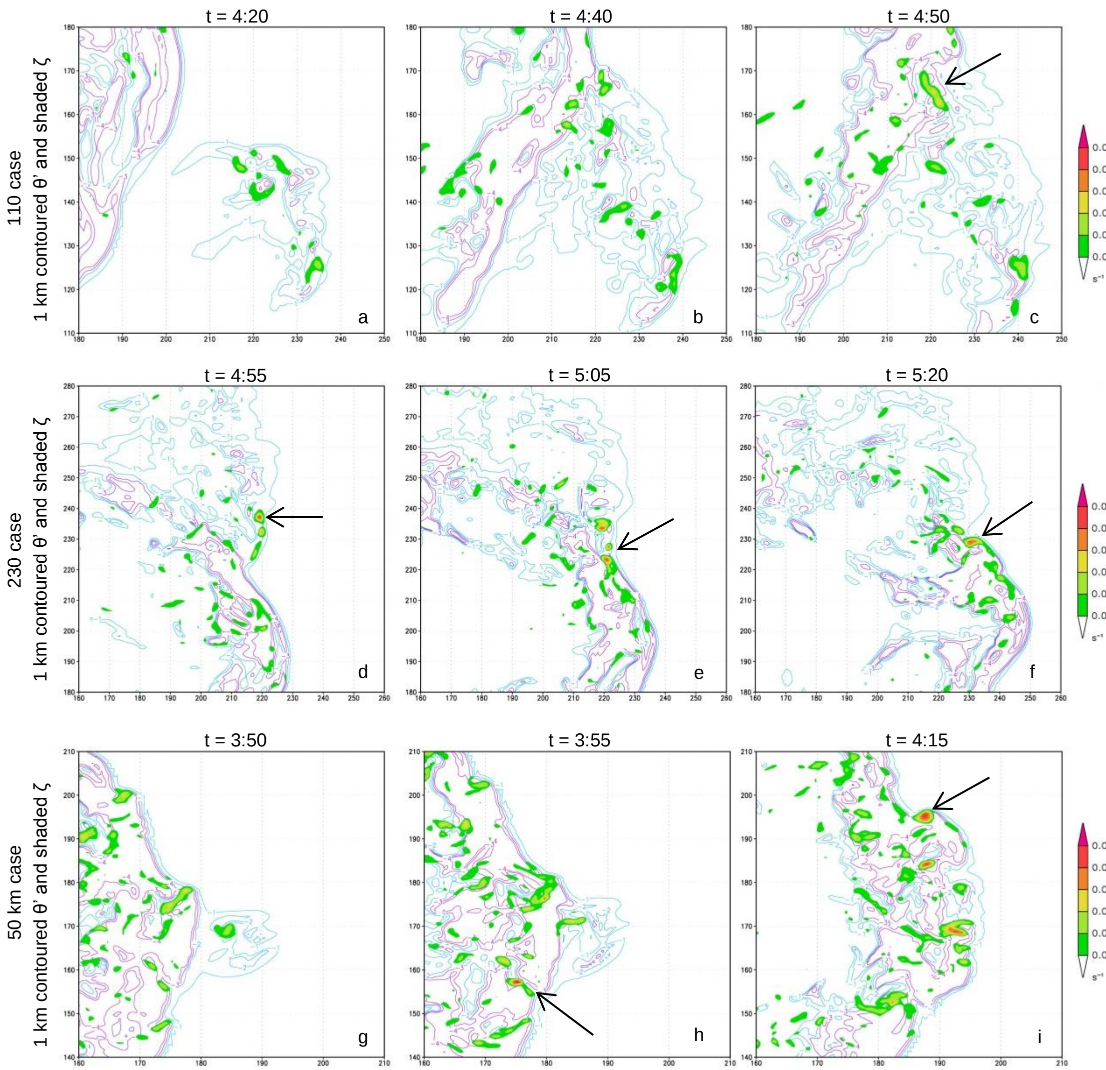

Figure 5: A time series of the 110 position case (a-c), 230 position case (d-f), and 50 km proximity case (g-i). These figures show the cold pool evolution, denoted by the contoured 1 km AGL potential temperature perturbations, and the mesovortex development, denoted by the shaded 1 km AGL vertical vorticity. The black arrows indicate regions of enhanced mesovortex development described in the text.

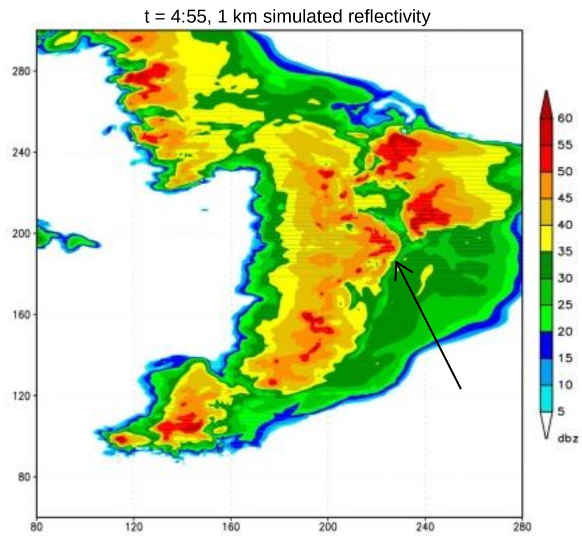

Figure 6: The 190 position case showing simulated radar reflectivity and an arrow denoting a distinct bowing segment of the convective region near the apex of the squall line.